Salt and cocrystals combining sulfathiazole with pyrimethamine

Journal:	*Crystal Growth & Design*
Manuscript ID	cg-2023-00626n
Manuscript Type:	Article
Date Submitted by the Author:	23-May-2023
Complete List of Authors:	Bodart, Laurie; Universite de Namur, Chemistry Body, Jeanne; Universite de Namur, Chemistry Tumanov, Nikolay; Universite de Namur, Department of Chemistry Leyssens, Tom; Universite catholique de Louvain, IMCN Wouters, Johan; Universite de Namur, Chemistry

Salt and cocrystals combining sulfathiazole with pyrimethamine

Laurie Bodart[§], Jeanne Body[§†], Nikolay Tumanov[§], Tom Leyssens[‡] and Johan Wouters[§]*

[§]Namur Medicine and Drug Innovation Center - Namur Research Institute for LIfe Science (NAMEDIC-NARILIS), Namur Institute of Structured Matter (NISM), Department of Chemistry, University of Namur (UNamur), 61 Rue de Bruxelles, B-5000 Namur, Belgium

[‡]Institute of Condensed Matter and Nanosciences, UCLouvain, 1 Place Louis Pasteur, B-1348 Louvain-la-Neuve, Belgium

KEYWORDS Pyrimethamine, sulfathiazole, cocrystal, salt, solvate, phase diagram, eutectic.

ABSTRACT Dihydrofolate reductase inhibitors such as pyrimethamine are known to have synergistic effects with sulfonamides. Four new solid forms combining pyrimethamine and sulfathiazole - one cocrystal (pyrimethamine-sulfathiazole (1:1)) and three solvated salt cocrystals (in which pyrimethamine and sulfathiazole are in a 1:2 molar ratio) are determined and

characterised. Desolvation of the salt cocrystals leads either to a physical mixture of the starting compounds or to the formation of the cocrystal (1:1) with an excess of sulfathiazole. The pyrimethamine sulfatiazole binary phase diagram was determined and reveals that the pyrimethamine sulfatiazole (1:2) composition point corresponds to a metastable eutectic. Obtaining this metastable eutectic as a pure powder is therefore rather difficult since it converts to a stable mixture of the (1:1) cocrystal + sulfathiazole. The above-mentioned drug-drug multicomponent systems are characterised in terms of thermal stability (by TGA/DSC) and solubility. Both pyrimethamine-sulfathiazole (1:1) cocrystal and pyrimethamine-sulfathiazole (1:2) ethanol solvated salt cocrystal result in an increase of the parent drugs solubility.

Introduction

The folic acid biosynthetic pathway is a common therapeutic target for antibacterials, antimicrobials and anticancer treatments.[1–4]

Among the enzymes of this metabolic route, two are of particular interest, namely dihydropteroate synthase (DHPS) and dihydrofolate reductase (DHFR). DHPS is found only in organisms that cannot uptake folate from their environment (mainly prokaryotes and lower

eukaryotes),[5] which makes this enzyme a good therapeutic target as it is not present in humans. In contrast, DHFR is found in all dividing cells (prokaryotes as well as eukaryotes). This enzyme produces tetrahydrofolate, a cofactor essential for cellular replication as it is implied in the synthesis of nucleic and amino acids.[4,5] Differences in the active site of bacterial and protozoal DHFR enzymes in comparison with human DHFR allow drug selectivity.[6] For example, pyrimethamine (**PYRM**, Fig. 1) is an antiprotozoal agent, trimethoprim is active on bacterial enzymes and methotrexate is used as human DHFR inhibitor for cancer treatment.[6,7]

Dihydrofolate reductase inhibitors are known to have synergic effects with dihydropteroate synthase inhibitors such as sulfa drugs. The most common combination, prepared as physical mixture, is probably trimethoprim/sulfamethoxazole (known as Bactrim) which is used as a treatment for, among others, urinary tract infections.[8,9] Other known combinations are pyrimethamine/sulfadoxine that was used to treat malaria[10] and pyrimethamine/sulfadiazine, which is used against toxoplasmosis.[11,12] Varde *et.al* have shown that trimethoprim/sulfadiazine combination is as effective as trimethoprim/sulfamethoxazole for the treatment of urinary tract infections and propose its use in case of sulfamethoxazole resistance.[13] This suggests that other combinations of DHFR and DHPS inhibitors could potentially overcome the problem of resistance.

Several DHFR inhibitors and sulfamides present a low solubility. For example, trimethoprim, sulfamethoxazole and sulfathiazole are classified as BCS class II drugs, meaning that they have a low solubility but a high permeability,[14,15] while data for pyrimethamine, sulfasalazine and sulfadiazine are not sufficiently clear to discriminate their classification as BCS class II or IV (low solubility and low permeability). Salt formation, cocrystallisation, solid-solution and eutectic preparation (among others) are techniques known to allow physico-chemical properties modulation (hygroscopy, stability, dissolution rate, solubility ...) of pharmaceutical compounds.[16-18] In consequence salt formation with DHFR inhibitors and sulfamides could be a valuable approach to modulate their solubility.

Despite its use in combination with sulfamides, on the 110 structures with pyrimethamin(e/ium) reported on the Cambridge Structural Database (CSD version 5.43 November 2022 update,[19]), only one solvated cocrystal of pyrimethamine with a sulfamide API (i.e. with sulfamethazine) is reported (CSD refcode KAXMEF[20]). Other salt structures are reported with saccharin, a sulfonamide derivative used as artificial sweetener.

Here are presented four new solid forms combining pyrimethamine with sulfathiazole, an antimycobacterial sulfa drug (Fig. 1). The solid forms combine **PYRM** with **STIAZ** under the form

of three solvated salt cocrystals (**PYRM$^+$-STIAZ$^-$-STIAZ-EtOH (1:1:1:0.5)**, **PYRM$^+$-STIAZ$^-$-STIAZ-iPrOH (1:1:1:0.5)** and **PYRM$^+$-STIAZ$^-$-STIAZ-MeCN (1:1:1:0.5)**) and one cocrystal (**PYRM-STIAZ (1:1)**). The binary phase diagrams between **PYRM** and **STIAZ** as well as the thermal stability of the four crystalline forms are reported. Water solubility of the non-solvated and ethanol solvated combinations is studied and compared to the one of the parent drugs.

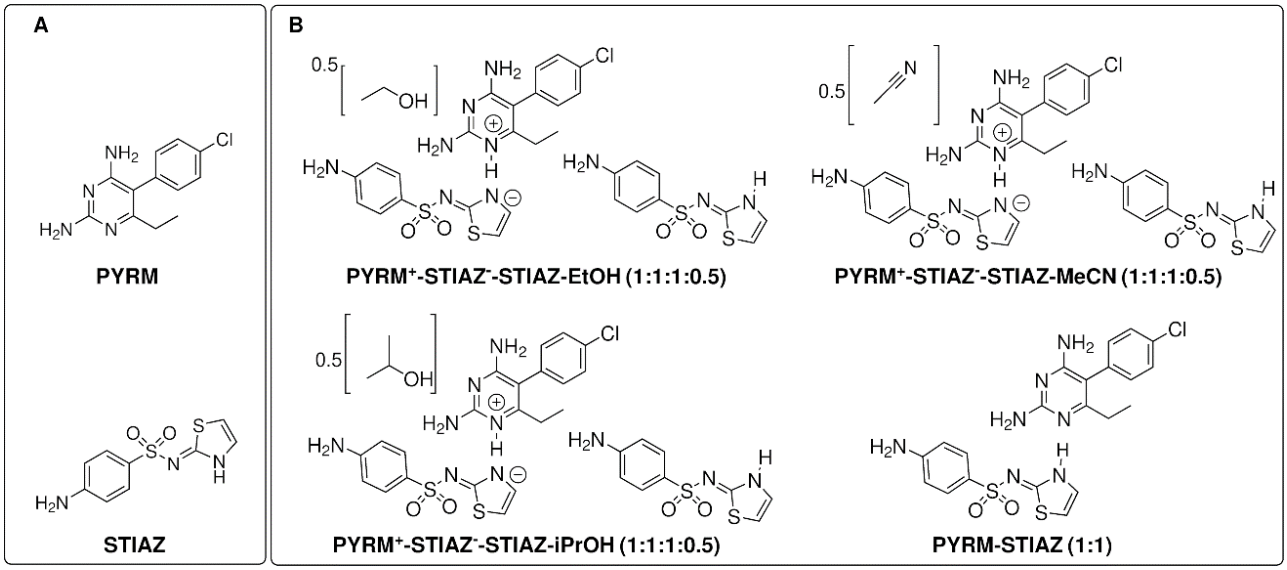

Figure 1. A: Chemical structures of parent APIs, pyrimethamine (**PYRM**) and sulfathiazole (**STIAZ**). B: Chemical structures of PYRM and STIAZ combinations; pyrimethaminium sulfathiazolate sulfathiazole ethanol solvated salt cocrystal (**PYRM$^+$-STIAZ$^-$-STIAZ-EtOH (1:1:1:0.5)**), pyrimethaminium sulfathiazolate sulfathiazole isopropanol solvated salt cocrystal (**PYRM$^+$-STIAZ$^-$-STIAZ-iPrOH (1:1:1:0.5)**), pyrimethaminium sulfathiazolate sulfathiazole acetonitrile solvated salt cocrystal (**PYRM$^+$-STIAZ$^-$-STIAZ-MeCN (1:1:1:0.5)**) and pyrimethamine sulfathiazole cocrystal (**PYRM-STIAZ (1:1)**).

Results and discussion

In this section, we first describe the structures of the solvated salt cocrystal and discuss their thermal behaviour. Then, the binary phase diagram between **PYRM** and **STIAZ** is established. Finally, we describe the crystal structure of the **PYRM-STIAZ (1:1)** cocrystal and discuss the solubility of **PYRM^{+}-STIAZ^{-}-STIAZ-EtOH (1:1:1:0.5)** and **PYRM-STIAZ (1:1)** in relation to that of the parent compounds.

Pyrimethaminium sulfathiazolate sulfathiazole solvated (EtOH, iPrOH or MeCN) salt cocrystals

Structural analysis

Liquid-assisted grinding in presence of EtOH (but not neat ball-milling) of pyrimethamine with sulfathiazole in 1:1 and 1:2 molar ratios leads to a new crystalline phase when grinding is performed in 2 mL eppendorfs plastic vials with seven stainless steel balls (2 mm of diameter) (Fig. S1). An excess of **PYRM** is identified on the powder pattern when ball-milling is done in equimolar quantities, which is not the case for the sample ground in 1:2 molar ratio (Fig. S1).

Recrystallisation of PYRM-STIAZ (1:2) powder (prepared by LAG EtOH) was performed by slow evaporation in EtOH.

Pyrimethaminium sulfathiazolate sulfathiazole ethanol solvated salt cocrystal (**PYRM$^+$STIAZ$^-$-STIAZ-EtOH (1:1:1:0.5)**) crystallises in P_{-1} space group (Table 1). The asymmetric unit contains one pyrimethaminium cation, one sulfathiazolate anion, one sulfathiazole molecule and a half molecule of EtOH (located near an inversion center). A proton transfer occurs from one **STIAZ** to **PYRM**. This proton transfer is confirmed by a decrease of the **STIAZ$^-$** C7 – N3 – C9 angle (111.2(2)˚, Fig. 2 and Table S3), which is closer to the value observed in sulfathiazolate (109.9(2)˚ in 2-methyl-4,5-dihydro-1H-imidazol-3-ium sulfathiazolate,[21] (CSD refcode: XIFPEI)) than to the one observed in sulfathiazole (C28 – N10 – C30 angle of 116.0(2)˚ in the sulfathiazole molecule in the structure, Fig. 2 and Table S3). This value is in accordance with the ones for sulfathiazole molecule (115.06-127(3) ˚ in polymorphs I to V of sulfathiazole (polymorph notation is given in Table S1 and is in accordance with the paper of Munroe *et al.*[22])).

Table 1. Experimental details.

	$PYRM^+$-$STIAZ^-$-STIAZ-EtOH (1:1:1:0.5)	**$PYRM^+$-$STIAZ^-$-STIAZ-iPrOH (1:1:1:0.5)**	**$PYRM^+$-$STIAZ^-$-STIAZ-MeCN (1:1:1:0.5)**	**PYRM-STIAZ (1:1)**
Chemical formula	$2(C_{12}H_{14}ClN_4^+)\cdot 2(C_9H_8N_3O_2S_2^-)\cdot 2(C_9H_9N_3O_2S_2)\cdot C_2H_6O$	$2(C_{12}H_{14}ClN_4^+)\cdot 2(C_9H_8N_3O_2S_2^-)\cdot 2(C_9H_9N_3O_2S_2)\cdot C_3H_8O$	$2(C_{12}H_{14}ClN_4^+)\cdot 2(C_9H_8N_3O_2S_2^-)\cdot 2(_9H_9N_3O_2S_2)\cdot C_2H_3N$	$C_{12}H_{13}ClN_4\cdot C_9H_9N_3O_2S_2$
Mr	1564.74	1578.77	1559.73	504.02
Crystal system, space group	Triclinic, $P\bar{1}$	Triclinic, $P\bar{1}$	Triclinic, $P\bar{1}$	Orthorhombic, *Pbca*
a, *b*, *c* (Å)	8.2895(2), 10.0115(2), 22.0236(5)	8.3290(2), 10.0742(3), 21.9489(5)	8.2767(2), 10.0027(2), 22.0661(5)	9.1931(1), 16.5708(2), 31.3944(3)
α, *β*, *γ* (°)	82.164(2), 83.671(2), 84.636(2)	81.784(2), 83.740(2), 84.762(2)	82.200(2), 82.939(2), 84.268(2)	90, 90, 90
V (Å^3)	1793.94(7)	1806.54(8)	1789.77(7)	4782.53(9)
Z	1	1	1	8
Radiation type	Cu *Kα*	Cu *Kα*	Cu *Kα*	Cu *Kα*
μ (mm^{-1})	3.57	3.55	3.57	3.33
Crystal size (mm)	0.09 × 0.06 × 0.05	0.28 × 0.23 × 0.03	0.21 × 0.16 × 0.03	0.28 × 0.15 × 0.11
Absorption correction	Analytical	Analytical	Analytical	Analytical
Tmin, *Tmax*	0.326, 0.850	0.587, 0.899	0.612, 0.911	0.560, 0.760
No. of measured, independent and observed [$I > 2\ \sigma(I)$] reflections	23732, 6343, 5930	16437, 6349, 5574	16074, 6317, 5494	15039, 4226, 3562
Rint	0.024	0.023	0.027	0.029
$(\sin\theta/\lambda)_{max}$ (Å^{-1})	0.598	0.597	0.598	0.597
$R[F^2 > 2\ \sigma(F^2)]$, $wR(F^2)$, *S*	0.035, 0.099, 1.07	0.036, 0.103, 1.04	0.035, 0.095, 1.03	0.042, 0.120, 1.04
No. of reflections	6343	6349	6317	4226
No. of parameters	502	512	501	361

No. of restraints	18	24	15	25
$\Delta\rho_{min}$, $\Delta\rho_{max}$ (e Å^{-3})	0.38, -0.45	0.34, -0.32	0.32, -0.33	0.27, -0.38

Experiments were carried out using an Oxford Diffraction Gemini Ultra R diffractometer. H atoms were treated by a mixture of independent and constrained refinement.

PYRM$^+$ interacts with **STIAZ$^-$** through H-bonds ($R_2^2(8)$, N4 — H···N2, N5$^+$ — H···N3$^-$ and D_1^1 (2), N7 — H···O2, Table S2 and Figs. 2(a) and (b)). **PYRM$^+$** dimers are stabilised by a $R_2^2(8)$ H-bond motif (N4 — H···N6, Table S2 and Figs. 2(b)). **PYRM$^+$** also interacts with **STIAZ** molecule through D_1^1 (2), N7 — H···N8 H-bonds (Table S2 and Figs. 2(a) and (b)).

Chains of sulfathiazolate anions along the *a*-axis are stabilised by $C_1^1(8)$ (N1 — H ··· O1) H-bonds (Fig. 2(d)). **STIAZ** molecules interact with sulfathiazolate anions through four D_1^1 (2) motifs (N1 — H ··· O4, N8 — H ··· N1, N8 — H ··· O2 and N1 — H ··· O3 (weak H-bond), Table S2 and Fig. 2(c)). Chains of **STIAZ$^-$** and **STIAZ** are stabilised through a $C_2^2(10)$ motif, resulting from the combination of $D_1^1(2)$, N8 — H ··· N1 and $D_1^1(2)$, N1 — H ··· O4 (Table S2 and Fig 2(e)). Dimers of **STIAZ** molecules are also observed ($R_2^2(8)$, N10 — H ··· N9, Table S2) in the structure of **PYRM$^+$-STIAZ$^-$-STIAZ-EtOH (1:1:1:0.5)**. Finally, EtOH molecules are H-bonded to **STIAZ$^-$** (O5 — H···N2, Table S2). The conformations of **STIAZ$^-$** and **STIAZ** are further stabilised through intramolecular chalogen bonds (C8 — S2···O1 and C29 — S4···O3, Table S2). Liquid-assisted

grinding of PYRM and STIAZ in 1:2 molar ratio in presence of iPrOH and MeCN leads to two new solvated cocrystals of salts that are isostructural to **PYRM^{+}-STIAZ^{-}-STIAZ-EtOH (1:1:1:0.5)** (Figs 3 and S1 and Tables 1 and S3).

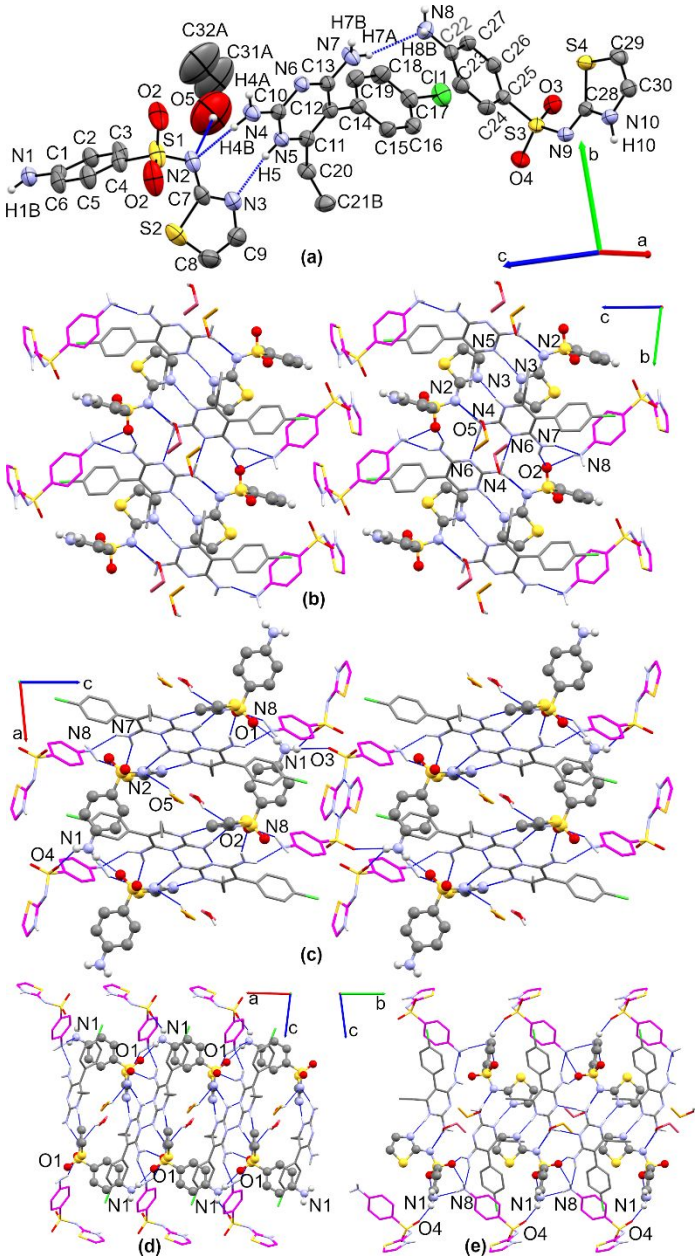

Figure 2. Ellipsoid plots (50% probability level) of **PYRM⁺-STIAZ⁻-STIAZ-EtOH (1:1:1:0.5)** (occupancy of EtOH is 0.5) (a), packing of **PYRM⁺-STIAZ⁻-STIAZ-EtOH (1:1:1:0.5)** along *a* and *b*-axes (b) and (c), **STIAZ⁻** form chains along *a*-axis (d), **STIAZ** and **STIAZ⁻** interact to form chains (e). Capped sticks representation of **PYRM⁺** in grey, of **STIAZ** molecule in magenta, of EtOH molecules in pink and orange (EtOH is disordered) and of **STIAZ⁻** anion in ball and stick style. H atoms not involved in H-bonds are not shown for clarity.

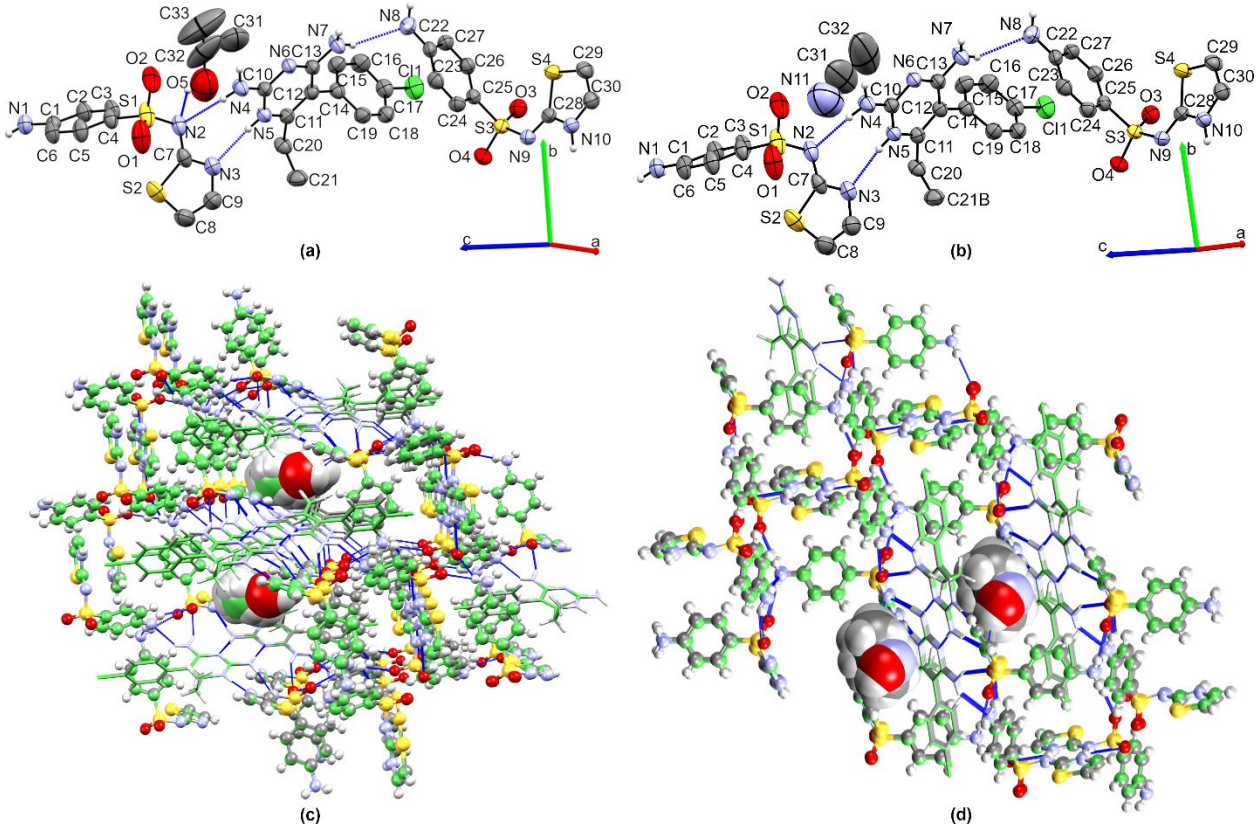

Figure 3. Ellipsoid plots (50% probability level) of **PYRM⁺-STIAZ⁻-STIAZ-iPrOH (1:1:1:0.5)** (a) and of **PYRM⁺-STIAZ⁻-STIAZ-MeCN (1:1:1:0.5)** (b), **PYRM⁺-STIAZ⁻-STIAZ-iPrOH (1:1:1:0.5)** and **PYRM⁺-STIAZ⁻-STIAZ-MeCN (1:1:1:0.5)** are isostructural to **PYRM⁺-STIAZ⁻-STIAZ-EtOH (1:1:1:0.5)** (c) and (d).

Thermal analysis and binary phase diagram

The **PYRM$^+$-STIAZ$^-$-STIAZ-EtOH (1:1:1:0.5)**, **PYRM$^+$-STIAZ$^-$-STIAZ-iPrOH (1:1:1:0.5)** and **PYRM$^+$-STIAZ$^-$-STIAZ-MeCN (1:1:1:0.5)** powders were analysed by TG/DSC (Fig. 4). Thermal analyses of these three isostructural solvated salts are very similar. All three powders present several thermal events between 145 and 165 ˚C, as well as two other endotherms at 188 ˚C and 209 ˚C (Table 2). TG analyses of the EtOH, iPrOH and MeCN solvated salt cocrystals indicate respectively a 3.0%, a 3.8% and a 2.2% weight loss between 140 and 160 ˚C, which can be associated with desolvation (theoretical mass losses of 2.9% EtOH, 3.8% iPrOH and 2.6% MeCN). It is interesting to note that one endothermic event is also observed at 176 ˚C on the DSC curve of **PYRM$^+$-STIAZ$^-$-STIAZ-MeCN (1:1:1:0.5)**, but not on the thermal analyses of the other solvated salt cocrystals. Variable-temperature PXRD analysis of **PYRM$^+$-STIAZ$^-$-STIAZ-EtOH (1:1:1:0.5)** reveals the formation of a physical mixture of pyrimethamine and polymorph I of sulfathiazole after desolvation at high-temperature (Fig. S2). However, heating can also lead to another outcome as the crystallisation of a new crystalline phase can occur (Fig. S3).

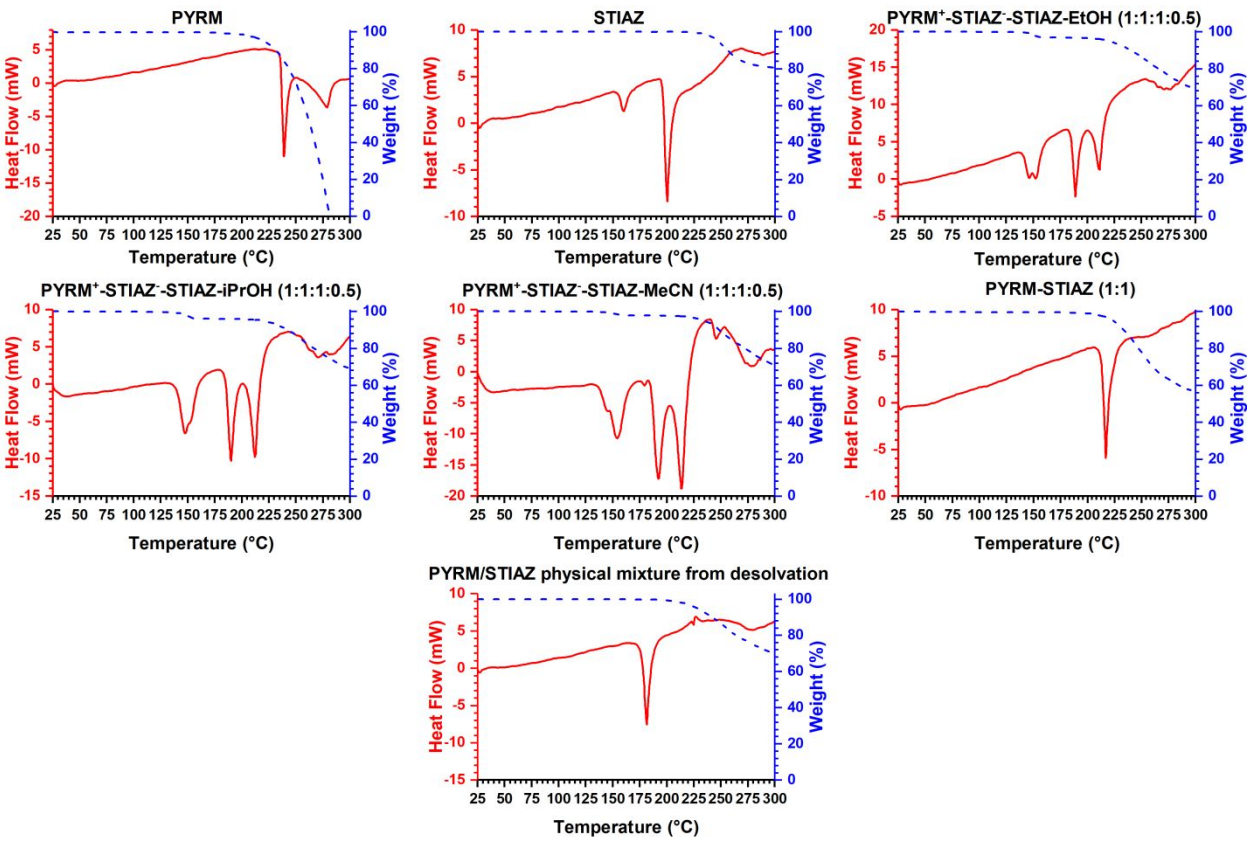

Figure 4. TG/DSC analysis of **PYRM**, **STIAZ**, **PYRM$^+$-STIAZ$^-$-STIAZ-EtOH (1:1:1:0.5)**, **PYRM$^+$-STIAZ$^-$-STIAZ-iPrOH (1:1:1:0.5)**, **PYRM$^+$-STIAZ$^-$-STIAZ-MeCN (1:1:1:0.5)** of **PYRM-STIAZ (1:1)** and of the PYRM/STIAZ (1:2) physical mix obtained from desolvation of **PYRM$^+$-STIAZ$^-$-STIAZ-EtOH (1:1:1:0.5)**. TGA curves in blue and DSC curves in red.

Furthermore, this new crystalline phase is also observed when the powder obtained from the variable-temperature PXRD experiment is re-analysed one month later (Fig. S3). Interestingly, in the powder pattern of the sample obtained after desolvation and crystallisation of this new crystalline phase, all PXRD peaks of STIAZ (polymorph I) are present, indicating an excess of

STIAZ. Combination of TG/DSC and PXRD analysis suggests that the new crystalline phase is a non-solvated compound in which the STIAZ:PYRM ratio is lower than 2.

To fully understand this behaviour and the endothermic events observed after desolvation, we determinated the PYRM/STIAZ binary phase diagram (Fig. 5). Solid samples (prepared by slurry of **PYRM** and/or **STIAZ** in **STIAZ** molar fraction ranging from 0 to 100%) were analysed by TG/DSC at a heating rate of 10 ˚C/min and 2 ˚C/min when overlapping events were suspected. Sulfathiazole exhibits a polymorphic transition at 164 ˚C between forms III (stable at low temperature) and I (stable at high temperature).[22] In this binary phase diagram we observe a stable peritectic at 213˚C which characterises the equilibrium between <PYRM-STIAZ (1:1)> and <PYRM> + liquid two-phase domain (non-congruent melting). A stable eutectic is observed between <PYRM-STIAZ (1:1)> and <STIAZ (I)> (90 mol% in STIAZ; 189˚C) characteristic of the equilibrium between <STIAZ (I) > + <PYRM-STIAZ (1:1)> two phase domain and the liquid phase. The liquidus line between this stable eutectic (90% STIAZ) and the melting point of **STIAZ (I)** (100% STIAZ) was extrapolated from the melting temperature of **STIAZ (I)** and the eutectic temperature. Indeed, at compositions between these two points, the eutectic invariant and the liquidus are too close in temperature to be distinguished by DSC. Finally, the physical mixture that

can be obtained by desolvation of solvated salt cocrystals, is characteristic of a metastable equilibrium between PYRM and STIAZ (dotted line in Figure 5, metastable eutectic point E': 66.6 mol% STIAZ, 176 ˚C).

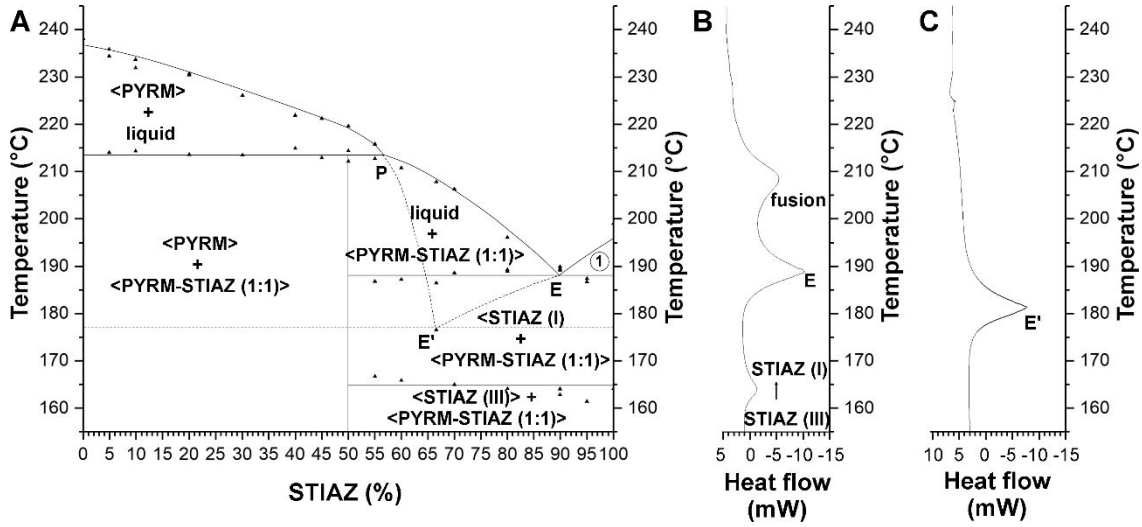

Figure 5. A: Binary phase diagram of PYRM and STIAZ. P, peritectic, E stable eutectic, E' metastable eutectic, ① <STIAZ (1)> + liquid. B: DSC curve of PYRM:STIAZ (30:70) and C: DSC curve of the metastable eutectic obtained upon desolvation of **PYRM^{+}STIAZ^{-}-STIAZ-EtOH (1:1:1:0.5)** at 170˚C.

Table 2. Correspondence of the thermal events observed on the DSC curves to the event on the binary phase diagram.

Phase	Desolvation & crystallisation (˚C)	Transition‡ (˚C)	Metastable eutectic§ (˚C)	Stable eutectic¶ (˚C)	Melting (˚C)
PYRM	/		/	/	239
STIAZ	/	164	/	/	199

PYRM$^+$-STIAZ$^-$-STIAZ-EtOH (1:1:1:0.5)	145-165	†	n.o.	188	209
PYRM$^+$-STIAZ$^-$-STIAZ-iPrOH (1:1:1:0.5)	145-165	†	n.o.	188	209
PYRM$^+$-STIAZ$^-$-STIAZ-MeCN (1:1:1:0.5)	145-165	†	176	188	209
PYRM-STIAZ (1:1)	/	/	/	213*	220

‡Transition: STIAZ polymorphic change, §metastable eutectic (66% STIAZ molar fraction): PYRM/STIAZ mixture that can be obtained from solvated salt cocrystal desolvation; ¶stable eutectic (90% STIAZ molar fraction): eutectic between the new crystalline phase PYRM-STIAZ (1:1) with STIAZ; †The transition overlaps with desolvatation but PXRD indicates that STIAZ polymorphic change occured; n.o.: not observed; *peritectic temperature.

Pyrimethamine sulfathiazole cocrystal

Structural analysis

On the binary phase diagram, a new crystalline phase (whose powder pattern matches with the one obtained upon desolvation of **PYRM$^+$-STIAZ$^-$-STIAZ-solvent (1:1:1:0.5)**) is identified with a composition close to PYRM/STIAZ (1:1). In order to determine the structure of this crystalline phase and confirm its composition, new neat grinding experiments were performed. Neat ball-milling in an Eppendorf leads only to physical mixture of PYRM and STIAZ (Figure S1), however,

more energetical grinding (in an agate jar) successfully leads to this new crystalline phase (Fig. S4). This phase is also reachable by slurry experiments performed in water.

Single-crystals obtained by recrystallisation of the PYRM:STIAZ 1:1 powder (neat grinding in agate jar) in ethyl acetate correspond to **PYRM-STIAZ (1:1)** cocrystal (Figure S4).

These results indicate that desolvation of the three solvated salt cocrystals can lead to the recrystallisation of an anhydrous cocrystal.

Pyrimethamine sulfathiazole cocrystal, **PYRM-STIAZ (1:1)**, crystallises in *Pbca* space group (Table 1). The asymmetric unit contains one pyrimethamine and one sulfathiazole molecule. No proton transfer occurs between **PYRM** and **STIAZ** as confirmed by the values of C10 — N5 — C11 angle (Fig. 6 (a)) of **PYRM** (117.2(2)˚), which is close to the one observed in neutral structures of **PYRM** (116.1(2) and 115.5(6)˚ (CSD refcodes: MUFMAB and MUFMAB01)). This is also confirmed by the value of the C7 — N3 — C8 angle (Fig. 6 (a)) in **STIAZ** (115.2(2)˚) which is closer to the ones observed in polymorphs I to V (115-127(3)˚) than in sulfathiazolate (109.9(2)˚ in 2-methyl-4,5-dihydro-1H-imidazol-3-ium sulfathiazolate,[21] (CSD refcode: XIFPEI)). **PYRM** and **STIAZ** interact through H-bonds ($R_2^2(8)$ motif, N4−H···N2 and N3−H···N5 and $D_1^1(2)$, N7 — H···O1) (Figure 6(a) and (b)). **PYRM** dimers are stabilised by a $R_2^2(8)$ motif (N4−H···N6) (Figure

6(b)). Chains of **STIAZ** along *b*-axis are stabilised through two $C_1^1(8)$ motifs (the first implies N1−H···O2 and the second implies N1−H···O1 H-bonds) (Figure 6(c)). Chains along *a*-axis are further stabilised through a $C_2^2(6)$ motif resulting from the combinations of the N1−H···O1 and the N1−H···O2 H-bonds (Figure 6(d)) as well as through a C7−S2···O2 intermolecular chalcogen bond (Figure 6(e)). **STIAZ** conformation is further stabilised by an intramolecular chalcogen bond (C9−S2···O2).

TG/DSC analysis of this cocrystal indicates melting at 213 ˚C (Table 2), which is followed by degradation as indicated by the weight loss observed on the TGA curve (Figure 4).

Thermodynamic solubility of the salts

Pyrimethamine and sulfathiazole are poorly soluble drugs. **STIAZ** is classified as BCS class II (low solubility but high permeability),[14,15] while data for pyrimethamine are not sufficiently clear to discriminate between BCS class II or IV (low solubility and permeability).[14] An HPLC method was used to assess the effect of salt formation/cocrystallisation of those compounds on their aqueous solubility. Parent drugs solubility was also evaluated.

Aqueous solubility of **PYRM**, **STIAZ (III)**, of their ethanol solvated salt cocrystal and of their non-solvated cocrystal was studied at 30 °C. Difference in solubility between **PYRM** and **STIAZ (III)** is quite important. Indeed, **PYRM** and **STIAZ** solubility are determined as 27 ± 1 mg/L and 595 ± 2 mg/L. These values are in accordance with literature data: 29.02 ± 2.69 mg/L at 37 °C[23] for **PYRM** and 594 mg/L[24] for **STIAZ**. Preparation of salts combining **PYRM** and **STIAZ** is thus expected to improve **PYRM** solubility as **STIAZ (III)** is over than ten times more soluble than **PYRM**.

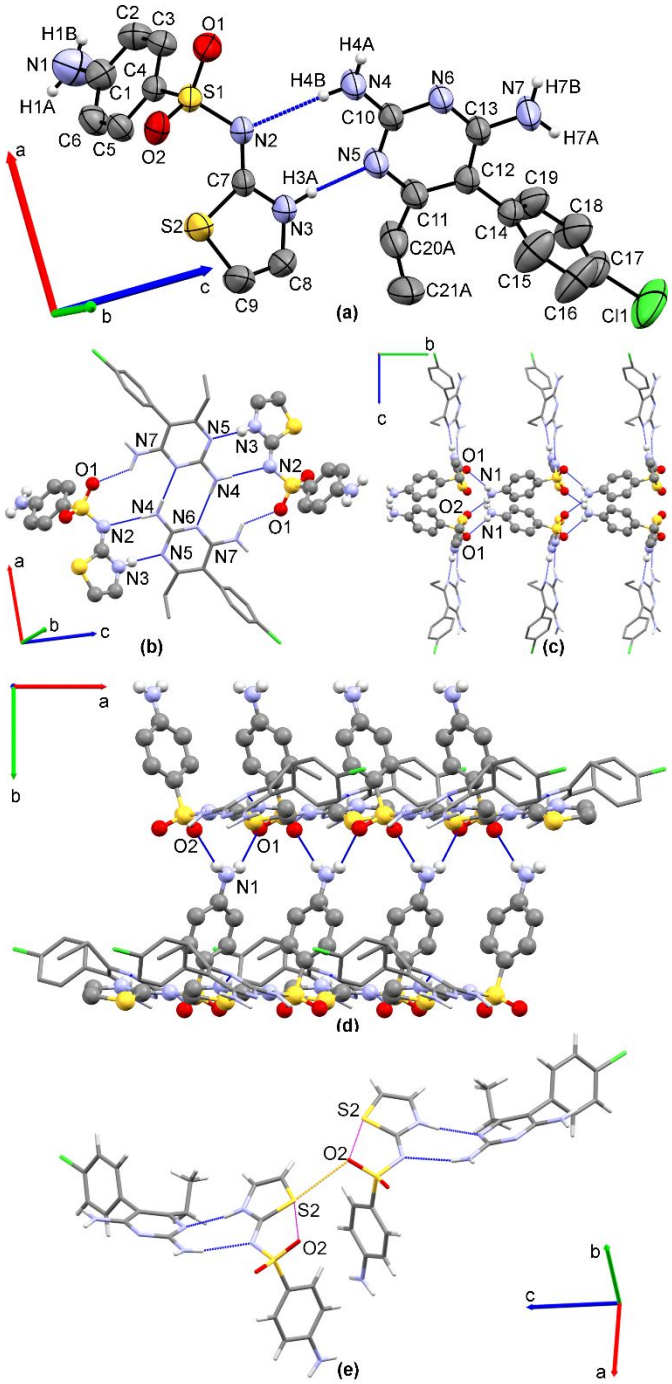

Figure 6. Ellipsoid plots (50% probability level) of **PYRM-STIAZ (1:1)** (a), **PYRM** dimers are stabilised through N4−H···N6 H-bonds (b), **STIAZ** chains along *b*-axis are stabilised by N1−H···O1 (first $C_1^1(8)$ motif) and N1−H···O2 H-bonds (second $C_1^1(8)$ motif) (c), STIAZ chains along *a*-axis are stabilised by N1−H···O1 and N1−H···O2 H-bonds ($C_2^2(6)$ motif) (d), and intra- as well as inter-molecular chalcogen bonds (magenta and orange dotted lines respectively) (e).

After 48h dispersion of **PYRM$^+$-STIAZ$^-$-STIAZ-EtOH (1:1:1:0.5)** in water, solubilised amounts of **PYRM** and **STIAZ** are 118 ± 5 (4.4-fold improvement) and 742 ± 7 mg/L (1.3-fold improvement) respectively (Fig. 7).

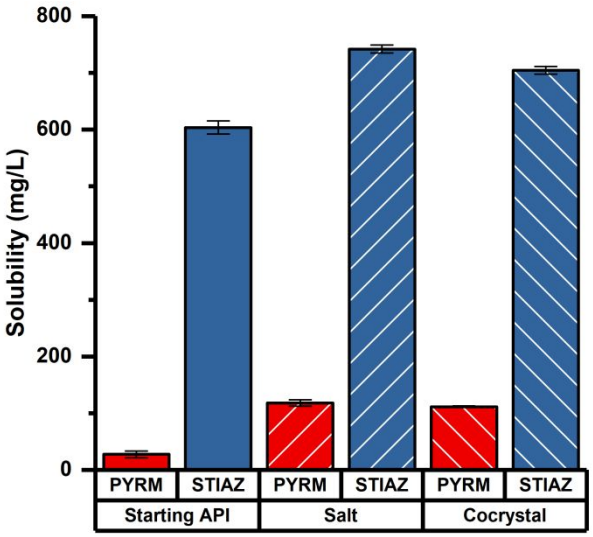

Figure 7. Solubility (at 30˚C) of **PYRM** (red) and **STIAZ** (blue) as starting APIs (plain columns) and when prepared as **PYRM$^+$-STIAZ$^-$-STIAZ-EtOH (1:1:1:0.5)** (salt, ascending white lines) and as **PYRM-STIAZ (1:1)** (cocrystal, descending white lines).

The 1:2 PYRM:STIAZ molar ratio is however not recovered in solution for **PYRM$^+$-STIAZ$^-$-STIAZ-EtOH (1:1:1:0.5)** (PYRM:STIAZ 14:86 instead of 33:66), Fig. S7. However, no change is observed on the PXRD pattern collected after solubility evaluation of **PYRM$^+$-STIAZ$^-$-STIAZ-EtOH (1:1:1:0.5)** (i.e. crystallisation of **PYRM-STIAZ (1:1)** is not observed). This could be

explained by two reasons. Firstly, the amount of **PYRM** that precipitates (calculated according to solubility data) is very low in comparison to the amount of powder initially immersed in water, and, secondly, the X-ray diffraction peaks of **PYRM** coincide with the ones of the solvated salt, making detection of a small amount of precipitated **PYRM** difficult. Furthermore, we do not exclude that the low amount of dissolved EtOH impacts these results.

Solubility of the **PYRM-STIAZ (1:1)** cocrystal was also determined at 30 ˚C and the results are similar to the one obtained from the **$PYRM^{+}$-$STIAZ^{-}$-STIAZ-EtOH (1:1:1:0.5)** solvated salt cocrystal. At this temperature, a 4.1-fold solubility increase (112 ± 1 *vs.* 27 ± 1 mg/L) is observed for **PYRM**, while **STIAZ** solubility is improved by a 1.2-fold (705 ± 5 *vs.* 595 ± 2 mg/L) (Fig. 7).

The 1:1 PYRM:STIAZ molar ratio is not recovered when this cocrystal is immersed in water (PYRM:STIAZ ratio is 14:86 in water, instead of 50:50). This suggests **PYRM** precipitation. The precipitated amount of **PYRM** is small in comparison to the amount of powder initially immersed in water. However, some X-ray diffraction peaks of **PYRM** (and notably the two most intense ones) do not correspond with the ones of the cocrystal. Two small peaks corresponding to the two most intense diffraction peaks of **PYRM** are effectively identified on the PXRD pattern collected

on recovered powder, indicating **PYRM** precipitation (Fig.S8). This result confirms the non-congruent solubility of the **PYRM-STIAZ (1:1)** cocrystal in water.

Despite **PYRM** partial precipitation, an increased amount of solubilised **PYRM** is detected after 48h immersion of **$PYRM^{+}$-$STIAZ^{-}$-STIAZ-EtOH (1:1:1:0.5)** or **PYRMSTIAZ (1:1)** in water. This indicates that preparation of **PYRM-STIAZ** multicomponent crystalline complexes (as a solvated salt cocrystal or as a cocrystal) allows an oversaturation of **PYRM** in solution with respect to pure PYRM.

Conclusions

Dihydropteroate synthase inhibitors and dihydrofolate reductase inhibitors are known to have synergistic biological activities. In this manuscript, four new multicomponent materials combining the dihydropteroate synthase inhibitor, sulfathiazole, with the dihydrofolate reductase inhibitor, pyrimethamine, are structurally described and characterised (thermal stability and aqueous solubility). Among those new multicomponent systems three solvated salt cocrystals (**$PYRM^{+}$-$STIAZ^{-}$-STIAZ-EtOH (1:1:1:0.5)**, **$PYRM^{+}$-$STIAZ^{-}$-STIAZ-iPrOH (1:1:1:0.5)** and **$PYRM^{+}$-$STIAZ^{-}$-STIAZ-MeCN (1:1:1:0.5)**), and one cocrystal (**PYRM-STIAZ (1:1)**) are identified.

The parent compounds used to prepare those multidrug systems are classified as BCS class II or IV, which is indicative of a low solubility. In this study, it is shown that the pyrimethaminium sulfathiazolate sulfathiazole ethanol solvated salt cocrystal (**PYRM^{+}STIAZ^{-}-STIAZ-EtOH (1:1:1:0.5)**) results in a 4.4-fold and 1.3-fold aqueous solubility increases for **PYRM** and **STIAZ** respectively (at 30˚C). Desolvation of this solvated salt cocrystal can lead to the formation of a physical mixture of **PYRM** and **STIAZ** (metastable state) or to a new crystalline phase, corresponding to a **PYRM-STIAZ (1:1)** cocrystal (stable state). The amount of **PYRM** and **STIAZ** released in water from this cocrystal was determined as 112 ± 1 mg/L (4.1-fold improvement) and 705 ± 5 mg/L (1.2-fold solubility increase) respectively.

If such combinations of those drugs in those ratios can lead to biological synergistic effects and/or improved bioavailability remains to be determined. However, the present study suggests cocrystallisation as a potential way for new dihydropteroate synthase and dihydrofolate reductase inhibitors drug-drug combinations.

Experimental

Materials

Pyrimethamine and sulfathiazole were respectively purchased from Sigma-Aldrich (Steinheim, Germany) and TCI Europe N.V. (Zwijndrecht, Belgium). Ethanol and ethylacetate were from Merck (Darmstadt, Germany) and were used without further purification. Acetonitrile, from Biosolve (Valkenswaard, Netherlands), and acetic acid, from Merck (Darmstadt, Germany), were HPLC grade and used without further purification.

Samples preparation

Pyrimethaminium sulfathiazolate sulfathiazole solvated salt cocrystal (**PYRM$^+$-STIAZ$^-$-STIAZ-EtOH (1:1:1:0.5)**, **PYRM$^+$-STIAZ$^-$-STIAZ-iPrOH (1:1:1:0.5)** and **PYRM$^+$-STIAZ$^-$-STIAZ-MeCN (1:1:1:0.5)**), are prepared by liquid-assisted grinding (LAG) in presence of EtOH, iPrOH or MeCN (for references about LAG, see reviews and papers of Friscic *et al.*, Shan *et al.*, Trask *et al.* and James *et al.*[25–28]). Samples consisting of pyrimethamine (75.0 mg, 0.302 mmol) with sulfathiazole (154.0 mg, 0.6032 mmol) are ground in Eppendorf^{TM} tubes, in presence of 30µL of EtOH, iPrOH or MeCN, using a Retsch MM 400 Mixer Mill apparatus (with seven stainless

steel balls of 2 mm diameter). **PYRM-STIAZ (1:1)** cocrystal is obtained by neat ball milling of PYRM (320.0 mg, 1.287 mmol) and STIAZ (328.5 mg, 1.287 mmol) in an agate grinding jar in presence of one bead agate ball (12 mm). Powder of this cocrystal can also be prepared by a slurry of an equimolar mixture of PYRM and STIAZ in water.

Single-crystals of **$PYRM^{+}$-$STIAZ^{-}$-STIAZ-EtOH (1:1:1:0.5)**, **$PYRM^{+}$-$STIAZ^{-}$STIAZ-iPrOH (1:1:1:0.5)** and **$PYRM^{+}$-$STIAZ^{-}$-STIAZ-MeCN (1:1:1:0.5)** are obtained by solvent evaporation crystallisation in EtOH, iPrOH and MeCN at room temperature (293-298 K). Crystals of **PYRM-STIAZ (1:1)** are obtained by crystallisation of the corresponding powder (prepared by neat ball milling) in EtOAc at room temperature (293-298 K).

Powder X-ray diffraction (PXRD)

Two diffractometers were used for powder diffraction data collection. The majority of PXRD data were collected in transmission mode at room temperature, with Cu $K\alpha_1$ radiation (λ = 1.54060Å) from 2 to 50° in 2θ angle on a STOE STADI MP diffractometer equipped with the MYTHEN2 linear detector .

Other PXRD data were collected with Cu $K\alpha$ radiation from 4 to 40° in 2θ angle using an X'PERT PRO PANalytical diffractometer in Bragg-Brentano geometry with the X'Celerator linear detector.

Variable-temperature powder diffraction data were collected with the X'PERT PRO PANalytical Bragg-Brentano diffractometer equipped with an Anton-Paar system. Data were collected at 25 ˚C, then from 40 to 170 ˚C and at 25 ˚C after cooling.

Thermogravimetric analysis (TGA) and differential scanning calorimetry (DSC)

TGA and DSC measurements were performed on a Mettler Toledo TGA/DSC 3+ apparatus. Solid samples (6-7 mg) were placed in open aluminium pans (100µL). Nitrogen (60 mL/min) was used as purge gas. Temperature range was 25 to 300 ˚C with a heating rate of 10 ˚C/min. Results were analysed using the STARe software, version 16.20.

PYRM/STIAZ binary phase diagram

To establish the binary phase diagram of PYRM/STIAZ, these two compounds were suspended and stirred (at 400 rpm) in water for 72 hours. Fifteen suspensions (molar fraction in STIAZ of 0,

5, 10, 20, 30, 40, 45, 50, 55, 60, 70, 80, 90, 95, 100) were prepared. The solids were recovered by evaporation of water at 60 ˚C and then analysed by PXRD to determine the nature of the crystalline phases. Each solid phase was then analysed by TG/DSC at a heating rate of 10 ˚C/min. When thermal events overlapped, the TG/DSC analysis was replicated at 2 ˚C/min. TGA and DSC measurements were performed on a Mettler Toledo TGA/DSC 3+ apparatus. Solid samples (6-7 mg) were placed in open (to observe TG events) and in pressed lids aluminium pans (100µL). Nitrogen (60 mL/min) was used as purge gas. Temperature range was 25 to 300 ˚C. Results were analysed using the STARe software, version 16.20.

Single-crystal X-ray diffraction (SCXRD)

Single-crystal X-ray diffraction data were collected on an Oxford Diffraction Gemini Ultra R system (four-circle kappa platform, Ruby CCD detector). Data were collected at 22 ˚C with Cu $K\alpha$ radiation (λ = 1.54184Å). Analytical absorption correction was performed using *CrysAlis* PRO.[29] Analytical numerical absorption correction was implemented using a multifaceted crystal model based on expressions derived by Clark & Reid[30] and then, empirical absorption correction was carried out using spherical harmonics[31] as implemented in the *SCALE3 ABSPACK* scaling

algorithm. All structures were solved using *SHELXT*[32] and then refined with *SHELXL-2018/1*[33] within *OLEX2*[34] and *shelXle*.[35]

Non-hydrogen atoms were refined anisotropically. Hydrogen atoms that were not involved in strong H-bond were refined as riding atoms (atomic displacement were fixed to 1.2 times (or 1.5 times for methyl groups) that of the parent atom). Hydrogen atoms involved in strong hydrogen bonds were located in difference Fourier maps (except for ethanol and isopropanol alcohol group in **PYRM$^+$-STIAZ$^-$-STIAZ-EtOH (1:1:1:0.5)** and **PYRM$^+$-STIAZ$^-$STIAZ-iPrOH (1:1:1:0.5)** because H-atom localisation in density difference maps was difficult due to solvent disorder).

CCDC deposition numbers for the reported structures are 2261393-2261398.

Search of the Cambridge Structural Database (CSD)

Known structures containing pyrimethamine were retrieved from the CSD version 5.43 November 2022 update,[19] using *ConQuest*.[36]

Crystal-packing comparison

Crystal-packing comparison was performed within *Mercury* [37] with the 'crystal-packing similarity' tool. Packing shell size was set to 15 molecules and angle and distance tolerance were set to 20˚ and 20% respectively. Comparison was also performed with structures containing sulfamide drugs other than sulfathiazole. In consequence, the smallest component was ignored and molecular difference and structure inversion were allowed. Bond types, H-atom positions, hydrogen count and bound count were ignored.

Determination of the aqueous solubility

Aqueous solubility of **PYRM**, **STIAZ**, **$PYRM^{+}$-$STIAZ^{-}$-STIAZ-EtOH (1:1:1:0.5)** and **PYRM-STIAZ (1:1)** cocrystal was evaluated in type I water (resistivity >18MΩ-cm and conductivity <0.056 $\mu S.cm^{-1}$) at 30 ˚C (Heidolf incubator 1000) by an HPLC method. First, a calibration curve was performed for each parent compound from seven solutions (with concentrations ranging from 215 to 2.5 µg/mL). Solubility was evaluated after agitation (900 rpm, Heidolf titramax 1000 platform shaker) of an excess of compound in type I water at 30 ˚C (samples were sonicated five minutes at the beginning of the experiment). After 48 hours of agitation, samples were centrifuged at 7000 rpm (eppendorf centrifuge 5430R, equipped with a FA-45-24-11 rotor) for five minutes.

The supernatant was collected, filtered on 0.2µm filters and diluted 50 times in a mixture of acetonitrile (MeCN), H_2O and acetic acid (HAc) (10/89.9/0.1 v/v/v) before injection in HPLC. Solubility was determined in triplicate. The remaining solid was analysed by high-resolution powder X-ray diffraction.

HPLC experiments were performed on an Agilent 1100 series HPLC system using UV detection at 280 nm. Separation of the analytes was achieved on an Agilent Zorbax-SB-Aq (3.5µm, 3.0×150 mm) using a gradient with mobile phase A (HAc 0.1% in H_2O) and mobile phase B (MeCN) at a flow rate of 0.5 mL/min. Gradient started at 10% B and linearly ramped up to 50% B in 10 minutes. This proportion was maintained for 3 minutes before returning to 10% B for 10 min re-equilibration. The injection volume was 5µL.

ASSOCIATED CONTENT

Supporting Information. The following files are available free of charge.

ESI contains a table retrieving sulfathiazole polymorphs notation and cell parameters, H-bond and chalcogen bond parameters as well as bond distances and angles of the described structures, experimental and calculated PXRD patterns of the described structures, variable-temperature

PXRD patterns and PXRD data of the compounds before and after solubility evaluation. (file type, PDF).

PYRM-STIAZ_combined.cif: crystallographic information files of the described structures (file type, CIF).

AUTHOR INFORMATION

Corresponding Author

* johan.wouters@unamur.be

Present Addresses

†UCB Pharma, Braine-l'Alleud, Belgium.

Author Contributions

The manuscript was written through contributions of all authors. All authors have given approval to the final version of the manuscript.

Funding Sources

This work was funded by the FNRS (PDR/OL T.0262.20).

ACKNOWLEDGMENT

The authors thank the PC^2 (Physico-Chemical Characterization) platform at the University of Namur for the use of XRD equipments. L.B. thanks the FNRS for funding (PDR/OL T.0262.20) and and Lionel Pochet for his help for the elaboration of the HPLC method.

ABBREVIATIONS

PYRM: pyrimethamine, STIAZ: sulfathiazole, SCXRD: single-crystal X-ray diffraction, PXRD: Powder X-ray diffraction, TGA: thermogravimetric analysis, DSC: differential scanning calorimetry, CSD: Cambridge structural database.

REFERENCES

(1) Swarbrick, J.; Iliades, P.; Simpson, J. S.; Macreadie, I. Folate Biosynthesis – Reappraisal of Old and Novel Targets in the Search for New Antimicrobials. *The Open Enzyme Inhibition Journal* 2008, *1*, 12–33.

(2) Murima, P.; Mckinney, J. D.; Pethe, K. Targeting Bacterial Central Metabolism for Drug Development. *Chemistry & Biology* 2014, *21*, 1423–1432.

(3) Winstanley, P. A.; Mberu, E. K.; Szwandt, I. S.; Breckenridge, A. M.; Watkins, W. M. In vitro activities of novel antifolate drug combinations against Plasmodium falciparum and human granulocyte CFUs. *Antimicrobial Agents and Chemotherapy* 1995, *39*, 948– 952.

(4) Gangjee, A.; Jain, H. D.; Phan, J.; Lin, X.; Song, X.; McGuire, J. J.; Kisliuk, R. L. Dual inhibitors of thymidylate synthase and dihydrofolate reductase as antitumor agents: design, synthesis, and biological evaluation of classical and nonclassical pyrrolo [2, 3-d] pyrimidine antifolates. *Journal of Medicinal Chemistry* 2006, *49*, 1055–1065.

(5) Bourne, C. R. Utility of the Biosynthetic Folate Pathway for Targets in Antimicrobial Discovery. *Antibiotics* 2014, *3*, 1–28.

(6) Schweitzer, B. I.; Dicker, A. P.; Bertino, J. R. Dihydrofolate reductase as a therapeutic target. *The FASEB Journal* 1990, *4*, 2441–2452.

(7) Sharma, M.; Chauhan, P. M. Dihydrofolate reductase as a therapeutic target for infectious diseases: opportunities and challenges. *Future Medicinal Chemistry* 2012, *4*, 1335–1365.

(8) Libecco, J. A.; Powell, K. R. Trimethoprim. *Pediatrics in Review* 2004, *25*, 375.

(9) Ho, J. M.-W.; Juurlink, D. N. Considerations when prescribing trimethoprim–sulfamethoxazole. *Cmaj* 2011, *183*, 1851–1858.

(10) Plowe, C. V.; Kublin, J. G.; Dzinjalamala, F. K.; Kamwendo, D. S.; Chimpeni, P.; Molyneux, M. E.; Taylor, T. E. Sustained clinical efficacy of sulfadoxine-pyrimethamine for uncomplicated falciparum malaria in Malawi after 10 years as first line treatment: five year prospective study. *Bmj* 2004, *328*, 545.

(11) Dannemann, B.; McCutchan, J. A.; Israelski, D.; Antoniskis, D.; Leport, C.; Luft, B.; Nussbaum, J.; Clumeck, N.; Morlat, P.; Chiu, J., et al. Treatment of toxoplasmic encephalitis in patients with AIDS: a randomized trial comparing pyrimethamine plus clindamycin to pyrimethamine plus sulfadiazine. *Annals of Internal Medicine* 1992, *116*, 33–43.

(12) Meneceur, P.; Bouldouyre, M.-A.; Aubert, D.; Villena, I.; Menotti, J.; Sauvage, V.; Garin, J.-F.; Derouin, F. In vitro susceptibility of various genotypic strains of Toxoplasma gondii to pyrimethamine, sulfadiazine, and atovaquone. *Antimicrobial Agents and Chemotherapy* 2008, *52*, 1269–1277.

(13) Varde, A.; Shetty, H.; Jadav, S.; Sheth, S.; Acharya, V.; Satoskar, R. Comparison of trimethoprim in combination with sulfadiazine or sulfamethoxazole in the treatment of urinary tract infections. *Journal of Postgraduate Medicine* 1981, *27*, 154.

(14) Lindenberg, M.; Kopp, S.; Dressman, J. B. Classification of orally administered drugs on the World Health Organization Model list of Essential Medicines according to the biopharmaceutics classification system. *European Journal of Pharmaceutics and Biopharmaceutics* 2004, *58*, 265 – 278, The International Association of Pharmaceutical Technology (APV).

(15) Gopi, S. P.; Ganguly, S.; Desiraju, G. R. A Drug–Drug Salt Hydrate of Norfloxacin and Sulfathiazole: Enhancement of in Vitro Biological Properties via Improved Physicochemical Properties. *Molecular Pharmaceutics* 2016, *13*, 3590–3594, PMID: 27580175.

(16) Sareen, S.; Mathew, G.; Joseph, L. Improvement in solubility of poor water-soluble drugs by solid dispersion. *International Journal of Pharmaceutical Investigation* 2012, *2*, 12.

(17) Savjani, K. T.; Gajjar, A. K.; Savjani, J. K. Drug solubility: importance and enhancement techniques. *ISRN Pharmaceutics* 2012, *2012*.

(18) Vimalson, D. C. Techniques to enhance solubility of hydrophobic drugs: An overview. *Asian Journal of Pharmaceutics (AJP): Free full text articles from Asian J Pharm* 2016, *10*.

(19) Groom, C. R.; Bruno, I. J.; Lightfoot, M. P.; Ward, S. C. feature articles The Cambridge Structural Database. *Acta Crystallographica B* 2016, *72*, 171–179.

(20) Alaa Eldin Refat, L.; O'Malley, C.; Simmie, J. M.; McArdle, P.; Erxleben, A. Differences in Coformer Interactions of the 2, 4-Diaminopyrimidines Pyrimethamine and Trimethoprim. *Crystal growth & design* 2022, *22*, 3163–3173.

(21) Coles, S. J.; Hursthouse, M. B.; Mayer, T. A.; Threlfall, T. L. 2-(4-Aminobenzenesulfonylamino)-3H-thiazol-1-ylium 2-Methyl-imidazolidine solvate. 2000; http://ecrystals.chem.soton.ac.uk/194/.

(22) Munroe, A.; Rasmuson, Å. C.; Hodnett, B. K.; Croker, D. M. Relative stabilities of the five polymorphs of sulfathiazole. *Crystal Growth & Design* 2012, *12*, 2825–2835.

(23) Badenhorst, L. Investigation of solubility and permeability of sulfadoxine and pyrimethamine mixtures. Ph.D. thesis, North-West University (South Africa), Potchefstroom Campus, 2017.

(24) Yalkowsky, S. H.; He, Y.; Jain, P. *Handbook of aqueous solubility data*; CRC press, 2016.

(25) Frišcic, T.; Childs, S. L.; Rizvi, S. A. A.; Jones, W. The role of solvent in mechanochemical and sonochemical cocrystal formation: a solubility-based approach for predicting cocrystallisation outcome. *CrystEngComm* 2009, *11*, 418–426.

(26) Shan, N.; Toda, F.; Jones, W. Mechanochemistry and co-crystal formation: Effect of solvent on reaction kinetics. *Chemical Communications* 2002, *2*, 2372–2373.

(27) Trask, A. V.; Motherwell, W. D. S.; Jones, W. Solvent-drop grinding: green polymorph control of cocrystallisation. *Chemical Communications* 2004, 890–891.

(28) James, S. L. et al. Mechanochemistry: opportunities for new and cleaner synthesis. *Chemical Society Reviews* 2012, *41*, 413–447.

(29) Rigaku Oxford Diffraction, CrysAlis PRO. *CrysAlis PRO* 2019, Rigaku Oxford Diffraction Ltd, Yarnton, England.

(30) Clark, R. C.; Reid, J. S. The Analytical Calculation of Absorption in Multifaceted Crystals. *Acta Crystallographica A* 1995, *51*, 887–897.

(31) Blessing, R. H. An Empirical Correction for Absorption Anisotropy. *Acta Crystallographica A* 1995, *51*, 33–38.

(32) Sheldrick, G. M. SHELXT - Integrated space-group and crystal-structure determination. *Acta Crystallographica A* 2015, *71*, 3–8.

(33) Sheldrick, G. M. Crystal structure refinement with SHELXL. *Acta Crystallographica C* 2015, *71*, 3–8.

(34) Dolomanov, O. V.; Bourhis, L. J.; Gildea, R. J.; Howard, J. A. K.; Puschmann, H. OLEX2: A complete structure solution, refinement and analysis program. *Journal of Applied Crystallography* 2009, *42*, 339–341.

(35) Hübschle, C. B.; Sheldrick, G. M.; Dittrich, B. ShelXle : a Qt graphical user interface for SHELXL. *Journal of Applied Crystallography* 2011, *44*, 1281–1284.

(36) Bruno, I. J.; Cole, J. C.; Edgington, P. R.; Kessler, M.; Macrae, C. F.; McCabe, P.; Pearson, J.; Taylor, R. New software for searching the Cambridge Structural Database and visualizing crystal structures. *Acta Crystallographica Section B: Structural Science* 2002, *58*, 389–397.

(37) Macrae, C. F.; Sovago, I.; Cottrell, S. J.; Galek, P. T.; McCabe, P.; Pidcock, E.; Platings, M.; Shields, G. P.; Stevens, J. S.; Towler, M., et al. Mercury 4.0: from visualization to analysis, design and prediction. *Journal of Applied Crystallography* 2020